RADIATIVE INTERACTIONS BETWEEN ABSORBING-EMITTING AND FLOWING MEDIA WITH INTERNAL ENERGY GENERATION

by John R. Howell

Lewis Research Center

Cleveland, Ohio

RADIATIVE INTERACTIONS BETWEEN ABSORBING-EMITTING AND

FLOWING MEDIA WITH INTERNAL ENERGY GENERATION

By John R. Howell

Lewis Research Center
Cleveland, Ohio

RADIATIVE INTERACTIONS BETWEEN ABSORBING-EMITTING AND

FLOWING MEDIA WITH INTERNAL ENERGY GENERATION

by John R. Howell

Lewis Research Center

SUMMARY

An analytical study of the local energy flux and emissive power in two adjacent regions is given. Each region is assigned a radiation absorption coefficient, mass flow rate, heat capacity, and volumetric energy source. The effect of these parameters and of the relative thickness of the regions is examined. The regions are assumed to be infinite, parallel layers of finite thickness in one case, and coaxial cylinders of finite radius in another. The problem of determining the local one-dimensional emissive power and radiant energy flux is solved by using a second-order diffusion solution with emissive power jump boundary conditions where applicable, and in the parameter ranges where such an approach is invalid a Monte Carlo transport analysis is used. The diffusion solution for the cases examined is accurate for optical thickness greater than about 1. The regions are assumed to be gray and have constant properties. A sample problem which demonstrates the use of the derived equations is presented.

INTRODUCTION

Radiative interchanges between adjacent absorbing-emitting media with different properties and internal energy sources are being examined because of applications to a number of practical systems. These systems include radiative shielding by injection of seeding material, radiative transfer in the gaseous-core nuclear propulsion system, and hypersonic shock phenomena. For many such problems, radiation is the major mechanism for energy exchange. The present work provides a simplified solution to radiative exchange problems where two distinct media are present. From this the engineer may estimate the importance of individual parameters on radiative transfer for his specific problem.

A diffusion solution including second-order terms and the effect of temperature slips

at region boundaries (ref. 1) is extended for use in two geometries. This type of approach leads to closed solutions in the form of algebraic equations and provides good accuracy over a very wide range of parameters (a much wider range than is generally conceded). Inclusion of the second-order and slip effects extends the results to most regions common to the problems mentioned previously. Certain regions do remain, however, where diffusion solutions are of doubtful validity or fail altogether. For this reason, a transport solution using a Monte Carlo technique (refs. 2 to 4) is utilized for determining where the diffusion solutions deviate appreciably from the more exact results.

All solutions, for both generality and simplicity, have the implicit assumptions of slug flow profiles, local thermodynamic equilibrium, no scattering, constant properties, and gray gases. In addition, the change in temperature with distance parallel to the flow direction is considered constant. Any or all of these may be very poor assumptions for a given problem, yet to remove any one of them gives a resulting loss of applicability to some problems otherwise covered. The assumption of a gray gas is a case in point. Various systems being considered, notably those involved in gaseous-core nuclear propulsion, might use small particle seeds to attain radiative absorption and can be analyzed on a gray gas basis, with some justification, so long as the wavelength of the radiation is not large compared with the particle size. Just as large a variety of problems, however, involve real gases where a gray gas assumption is simply incorrect. To allow solution of any of this latter class would probably mean a specialized approach to the exclusion of many related problems. For this reason, the assumptions are included, with the caution that use of the equations presented herein implies a responsible look by the user at the assumptions involved.

SYMBOLS

A area

C_p heat capacity

D ratio of plane region thicknesses, L_1/L_2

D_c ratio of cylinder diameters, D_1/D_2

E radiant energy per unit time

e emissive power, σT^4

e_λ spectral blackbody energy distribution (spectral emissive power)

I mean square absorption coefficient defined by eq. (A12)

L dimension in z direction

ℓ region thickness

Q	volumetric energy generation rate
q	energy flux
R	dimensionless radius, r/R_2
r	radial cylindrical coordinate
T	absolute temperature
u	velocity of flow
V	volume
x	Cartesian coordinate in flow direction
y	Cartesian coordinate perpendicular to x and z
Z	dimensionless coordinate, z/L_2
z	Cartesian coordinate normal to bounding plane
Γ	total energy sources per unit volume, $-\rho C_p u(dT/dx) + Q$
ϵ	emissivity of bounding surfaces
κ	gas absorption coefficient
κ_R	Rosseland mean gas absorption coefficient, eq. (A10)
κ_s	mean absorption coefficient, eq. (A11)
ρ	density
σ	Stefan-Boltzmann constant
τ	optical thickness, $\kappa\ell$
$\varphi(D)$	$\varphi(Z)$ evaluated at $Z = D$
$\varphi(R)$	dimensionless local emissive power for concentric cylinders, $[e(R) - e_w]/\Gamma_1 R_1$
$\varphi(Z)$	dimensionless local emissive power for parallel planes, $[e(Z) - e_w]/\Gamma_1 L_1$
$\psi(D)$	$\psi(Z)$ evaluated at $Z = D$
$\psi(R)$	dimensionless energy flux in concentric cylinders, $-q/\Gamma_1 R_1$
$\psi(Z)$	dimensionless energy flux in parallel planes, $-q/\Gamma_1 L_1$
Ω	function defined by eq. (A4)
ω	solid angle

Subscripts:

D	evaluated at $Z = D$

g   gas

g-g   dimensionless gas interface slip condition

g-w   dimensionless wall slip condition

g,w   evaluated in gas very close to wall

w   bounding wall black emissive power

x   in x-direction

z   in z-direction

λ spectral value

0   origin for Taylor series expansion

1   region 1

2   region 2

(a) Parallel regions.

(b) Concentric cylindrical regions.

Figure 1. – Flow models.

ANALYSIS

The diffusion equations for the radiative interchange between two adjacent absorbing-emitting regions are derived in the appendix, and the resulting equations for the local emissive power and radiant flux are summarized in this section. Two geometries are examined.

The first arrangement consists of two parallel planes of finite thickness as shown in figure 1(a). The interface between the regions is assumed to be an imaginary plane across which no mixing occurs and which offers no resistance to radiative energy transfer. The outer boundary of region 2 $(z = L_2)$ is assumed to be a solid gray wall of emissivity ϵ. The inner boundary of region 1 $(z = 0)$ is taken to be a plane across which there is no net radiative flux. The two planes examined here may then be viewed as one-half of a symmetrical system made up of a central or core region flanked by two
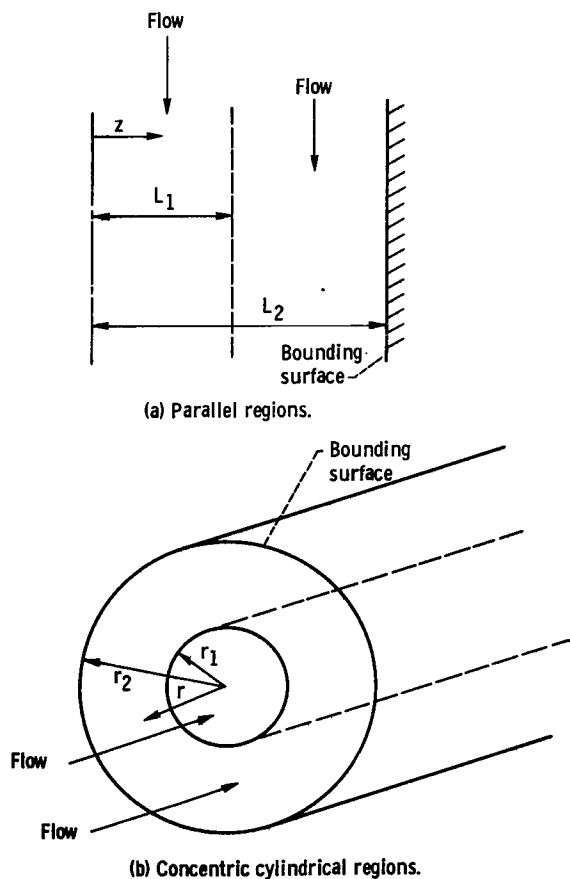
identical regions with properties differing from the core.

The second geometry is shown in figure 1(b) and consists of two concentric regions of absorbing-emitting media bounded on the outer surface ($r = r_2$) by a solid boundary of emissivity ϵ. The interface between the regions is an imaginary cylindrical surface assumed to have no radial mixing occurring across it and offering no resistance to radiative transfer.

Diffusion Solution

Parallel plane geometry. - In the appendix, the second-order diffusion solution as proposed by Deissler (ref. 1) is used to determine the one-dimensional emissive power distribution for the two cases. First, the parallel layer geometry (fig. 1(a)) with slug flow traveling parallel to the boundaries and with constant and uniform internal energy generation in each region is examined. Individual absorption coefficients for radiation, κ_1 and κ_2, are present in regions 1 and 2, respectively. If the dimensionless parameters are defined as

$$\varphi(Z) = \frac{e_g(Z) - e_w}{\Gamma_1 L_1}$$

$$Z = \frac{z}{L_2}$$

$$D = \frac{L_1}{L_2}$$

$$\tau_1 = \kappa_1 L_1$$

$$\tau_2 = \kappa_2(L_2 - L_1)$$

$$\Gamma = -\rho C_p u \frac{dT}{dx} + Q$$

then the emissive powers in regions 1 and 2 at point Z are given by equations (A29) and (A26) of the appendix, respectively, which are

$$\varphi_1(Z) - \delta\varphi_{g-w} = \varphi_2(D) - \delta\varphi_{g-w} + \frac{3\tau_1}{8D^2}(D^2 - Z^2) + \delta\varphi_{g-g} \qquad 0 \leq Z \leq D \qquad \text{(A29)}$$

and

$$\varphi_2(Z) - \delta\varphi_{g-w} = \frac{3\tau_2(\Gamma_2/\Gamma_1)(1 - Z^2)}{8D(1 - D)} + \frac{3\tau_2}{4(1 - D)}\left(1 - \frac{\Gamma_2}{\Gamma_1}\right)(1 - Z) \qquad D \leq Z \leq 1 \qquad \text{(A26)}$$

where the slip values across the gas-wall and gas-gas interfaces ($\delta\varphi_{g-w}$ and $\delta\varphi_{g-g}$, respectively) are given by

$$\delta\varphi_{g-w} = \left(\frac{1}{\epsilon} - \frac{1}{2}\right)\left(\frac{1 - D}{D}\frac{\Gamma_2}{\Gamma_1} + 1\right) + \frac{3(\Gamma_2/\Gamma_1)(1 - D)}{8D\tau_2} \qquad \text{(A27)}$$

and

$$\delta\varphi_{g-g} = \frac{3}{8D}\left(\frac{D}{\tau_1} - \frac{1 - D}{\tau_2}\frac{\Gamma_2}{\Gamma_1}\right) \qquad \text{(A28a)}$$

Equation (A29) shows that the local dimensionless emissive power of the gas in region 1 depends on the emissive power in region 2 evaluated at the boundary between the regions, the relative thickness D, the optical thickness τ_1, and $\delta\varphi_{g-g}$. The last term accounts for the discontinuity in emissive power that occurs at the boundary between absorbing-emitting regions with internal sources (refs. 5 and 6).

The local emissive power in region 2 depends on the optical thickness τ_2 in region 2, the relative thickness D of the layers, and the ratio of sources in the two regions Γ_2/Γ_1. In addition, there is a dependence on the emissive power discontinuity at the bounding surface $\delta\varphi_{g-w}$, which, in turn, depends on the same parameters and the wall emissivity ϵ.

The local radiative flux in a direction normal to the slab boundaries is given by equations (A36) and (A35) in the appendix as

$$\psi_1(Z) = \frac{Z}{D} \qquad 0 \leq Z \leq D \qquad \text{(A36)}$$

6

$$\psi_2(Z) = 1 + \frac{\Gamma_2}{\Gamma_1}\left(\frac{Z}{D} - 1\right) \qquad D \le Z \le 1 \tag{A35}$$

where $\psi(Z)$ is a nondimensional radiative flux given by

$$\psi(Z) = -\frac{q(Z)}{\Gamma_1 L_1}$$

Concentric cylindrical geometry. - It is also shown by equations (A40) to (A43) in the appendix that, for the geometric model shown in figure 1(b), the emissive power distribution radially is given by

$$\varphi_1(R) - \delta\varphi_{g-w} = \varphi_2(D_c) - \delta\varphi_{g-w} + \delta\varphi_{g-g} + \frac{3\tau_1}{16}\frac{D_c^2 - R^2}{D_c^2} \qquad 0 \le R \le D_c \tag{A40}$$

and

$$\varphi_2(R) - \delta\varphi_{g-w} = \frac{3\tau_2}{16}\frac{\Gamma_2}{\Gamma_1}\frac{1 - R^2}{D_c(1 - D_c)} - \frac{3\tau_2 D_c}{8(1 - D_c)}\left(1 - \frac{\Gamma_2}{\Gamma_1}\right)\ln R \qquad D_c \le R \le 1 \tag{A41}$$

where

$$\delta\varphi_{g-w} = \frac{1}{2}\left(\frac{1}{\epsilon} - \frac{1}{2}\right)\left(\frac{\Gamma_2}{\Gamma_1}\frac{1 - D_c^2}{D_c} + D_c\right) + \frac{3}{16}\frac{1 - D_c}{\tau_2}\left(\frac{\Gamma_2}{\Gamma_1}\frac{1 + D_c^2}{D_c} - D_c\right) \tag{A42}$$

and

$$\delta\varphi_{g-g} = \frac{9}{32D_c}\left[\frac{D_c}{\tau_1} - \frac{1}{3}\frac{1 - D_c}{\tau_2}\left(4\frac{\Gamma_2}{\Gamma_1} - 1\right)\right] \tag{A43}$$

The dimensionless variables have the same physical interpretation as before, but now they have slightly different forms in some cases to reflect the difference in geometry. The variables are

$$\varphi(R) = \frac{e_g(R) - e_w}{\Gamma_1 r_1}$$

$$D_c = \frac{r_1}{r_2}$$

$$\tau_1 = \kappa_1 r_1$$

$$\tau_2 = \kappa_2(r_2 - r_1)$$

$$R = \frac{r}{r_2}$$

The local radial radiative flux is given by equations (A44) and (A45) as

$$\psi_1(R) = \frac{R}{2D_c} \qquad 0 \leq R \leq D_c \tag{A44}$$

and

$$\psi_2(R) = \frac{D_c}{2R} + \frac{\Gamma_2}{\Gamma_1} \frac{R^2 - D_c^2}{2RD_c} \qquad D_c \leq R \leq 1 \tag{A45}$$

where

$$\psi(R) = -\frac{q(R)}{\Gamma_1 r_1}$$

Monte Carlo Transport Solution

For comparison with the diffusion solutions presented in the preceding sections, a transport analysis was made by means of Monte Carlo techniques. For the parallel plane geometry, the essential equations and concepts are available in reference 2. For the cylindrical case, similar information is available in reference 3, and a general discus-

8

sion of Monte Carlo approaches to radiative transfer problems is presented in reference 4.

Because of the need to define volume elements for determining local values of gas emissive power, it is not feasible to determine the gas emissive power exactly at the gas-wall boundary. Therefore, it is assumed in the Monte Carlo solutions presented herein that the emissive power slip at the wall could be adequately represented by extrapolation of the radial gas emissive power curve to the wall from the three calculated $\varphi_2(Z)$ points in the gas adjacent to the wall.

Because the Monte Carlo technique involves the sampling of a model of the radiant energy exchange process by statistical means, the answers obtained contain statistical fluctuations. Some estimate of the probable error in the results is desirable. The 95-percent confidence limits on the Monte Carlo points are therefore used to indicate that the value of the point has a probability of 95 percent of lying within the range shown. The limits did not usually exceed the size of the symbols used to plot the points. Where they did, the limits are indicated by vertical bars.

RESULTS

Comparison is now made of the diffusion and transport solutions to determine the range of parameters for which the diffusion solution is valid. It is expected from the assumptions inherent in the diffusion approach that diffusion results would be most in error for small values of τ and in regions within one mean free path of a boundary.

Parallel Planes

In figure 2, both regions are given identical properties and equal widths (D = 0.5). The effect of optical thickness on the emissive power distribution is then demonstrated. Accuracy of the diffusion solution on a percentage difference basis is seen to be excellent above $\tau \approx 2$ and
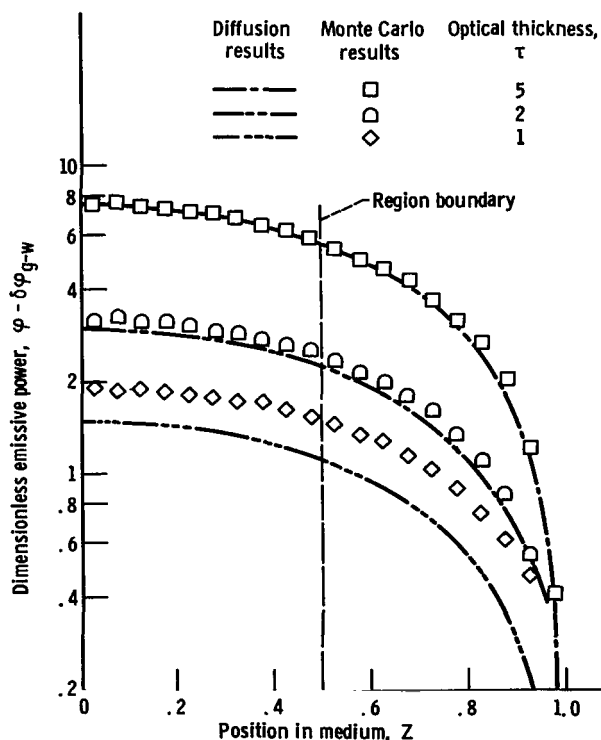
Figure 2. - Dimensionless gas emissive power distribution in gray planes. Ratio of energy sources, 1; ratio of thicknesses, 0.5; optical thickness in region 1 same as in region 2.

Diffusion results	Monte Carlo results	Optical thickness, τ
—·—	□	5
—··—	⌂	2
—···—	◇	1

9

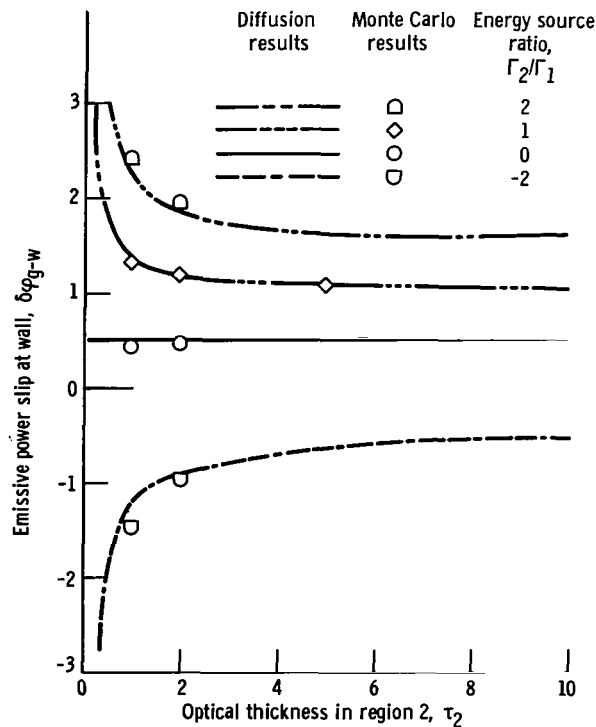| Diffusion results	Monte Carlo results	Energy source ratio, Γ_2/Γ_1
— — — —	◻	2
—————— —	◇	1
——————	◯	0
— · — · —	◻	-2

Figure 3. - Effect of optical thickness on radiation slip. Ratio of thicknesses, 0.5; optical thickness in region 1 same as in region 2.
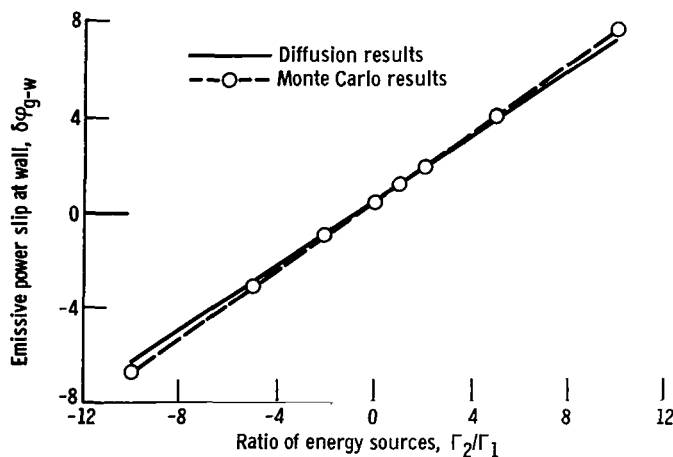

Figure 4. - Effect of energy source ratio on emissive power slip at wall in parallel plane regions. Optical thickness in region 1, 2; optical thickness in region 2, 2; thickness ratio, 0.5.

acceptable at even smaller values of τ.

In figure 3, the emissive power slip at the solid boundary is shown as a function of gas optical thickness in region 2, with the ratio of energy source strengths as a parameter. Again, accuracy is quite good for the diffusion solution at $\tau_2 = 2$ and appears to diverge from the Monte Carlo results below this value. Even at $\tau_2 = 1$, however, the errors between the results are small. It should be noted that the equation for $\delta\varphi_{g-w}$ by the diffusion approach does not depend on the energy reaching the bounding surface from region 1. Yet, for a very small τ_2, it would be expected that $\delta\varphi_{g-w}$ would depend chiefly on that energy, so that certain combinations of parameters might lead to more error in $\delta\varphi_{g-w}$ than is implied in figure 3.

In figures 3, 5, 8, and 10, the source strength ratio Γ_2/Γ_1 appears as a parameter. The definition of Γ is the net volumetric rate of energy accumulation due to both internal energy generation and change in the enthalpy of the media. If the flow conditions of the media are such that the enthalpy term is greater than the energy generation term, then it is quite possible for Γ to have negative values in one or both regions. This simply means a net volumetric energy sink is present in the region. Both positive and negative ratios of source strengths are therefore shown.
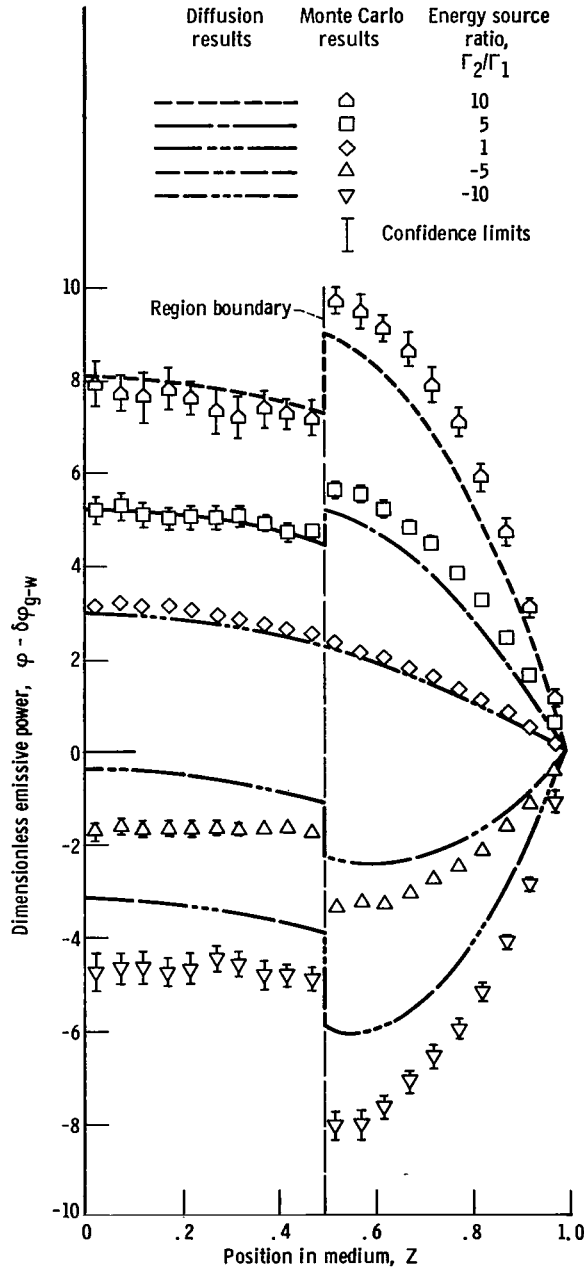
The effect of the energy source

Figure 5. - Effect of energy source ratio on emissive power. Optical thickness in region 1, 2; optical thickness in region 2, 2; thickness ratio, 0.5.

ratio of the regions Γ_1/Γ_2 on the emissive power slip at the wall is demonstrated in figure 4. Three results are noted. First, the difference between the diffusion and Monte Carlo results increases as the absolute magnitude of Γ_2/Γ_1 increases. Second, the absolute magnitude of the slip itself increases. Third, the percentage difference between the two solutions does not change markedly as the source ratio becomes large.

Figure 5 shows the emissive power distributions with the slip value subtracted out to avoid a greatly expanded scale. This is valid because both methods were shown to predict accurately the wall slip in emissive power. Therefore, it is evident that large energy source ratios give larger differences between the solutions. However, if the slip values are added back in, the percentage difference between the solutions is not a function of source ratio, as far as can be determined. This trend continues out to source ratios of plus and minus 10^{10} (for which results are not presented). This subtraction of the slip values also accounts for the apparent dependence of the percentage difference on the sign of Γ_2/Γ_1 which does not appear if the slip is added to the results.

It is interesting to note the emissive power jumps at the region boundary. The magnitude of these jumps increases with increasing magnitude of source strength ratios. This is in accord with the results of reference 6.

The remaining parameter to be examined is the slab thickness ratio D. The effect on φ (at two positions) of varying this parameter while holding all other conditions in the re-
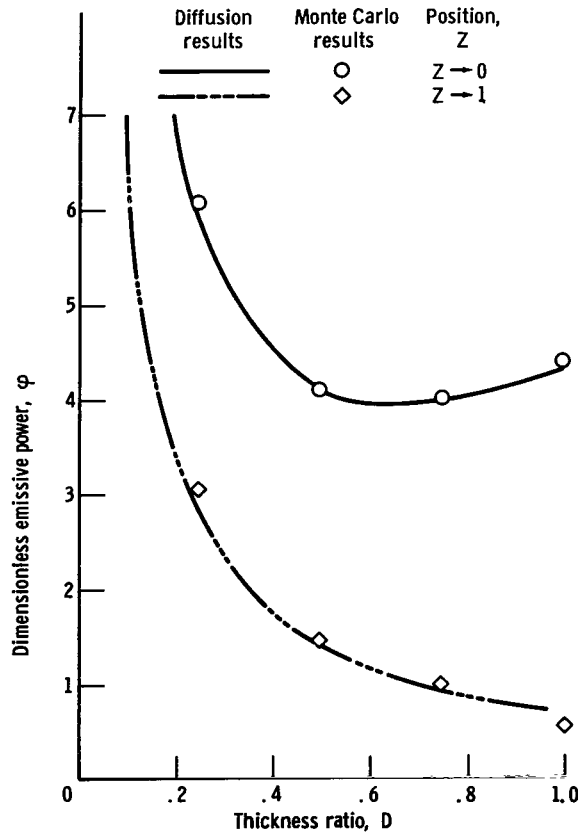
Diffusion results	Monte Carlo results	Position, Z
——————	○	$Z \to 0$
— — — —	◇	$Z \to 1$

Figure 6. - Effect of plane region thickness on emissive power. Energy source ratio, 1; optical thickness in region 1, $10D$, where D is thickness ratio; optical thickness in region 2, $2(1 - D)$.

gions constant is shown in figure 6 for one case. The absorption coefficients κ_1 and κ_2 are constant, so that τ_1 and τ_2 are now functions of D. It is seen that for intermediate D values good agreement between solutions is reached. This is expected because the diffusion solution, even including the emissive power jump at the bounding surface, becomes inaccurate within a radiation mean free path of a boundary. The best agreement should occur for $\tau_2 = \tau_1$, which is the case at D = 1/6. It is difficult from the results given to determine whether this is the case. It is interesting that for values of D $\approx$ 1, the diffusion solution will give a slip prediction (eq. (A27)) based only on ϵ and τ_2, while in actuality the slip for D $\approx$ 1 should be a function also of conditions in region 1 as the optical thickness of region 2 becomes small. This is why $\varphi_2(Z \to 1)$ for the diffusion solution begins to diverge from the Monte Carlo analysis as D approaches 1 in figure 6.

For the parallel plane geometry, then, the greatest inaccuracies in the diffusion results occur for small τ, or for D near 0 or 1. This would be predicted a priori from knowledge of the assumptions inherent in the diffusion approach. What is surprising is that the errors are of the order of a few percent even for $\tau \approx 1$ and for extremal values of D.

In figures 7 to 11, an analogous set of results is presented for the case of concentric regions as shown in figure 1(b). The conclusions remain the same as for parallel regions, in that the accuracy of the diffusion solution is very good for all the cases examined. Accuracy for like values of parameters is slightly inferior to the results for parallel regions.

Sample Problem

To illustrate the use of the diffusion solution in a more practical calculation, the radial temperature distribution in a coaxial-flow gaseous-core nuclear propulsion system will be determined. Such a device consists of a core of fissionable material in the gase-
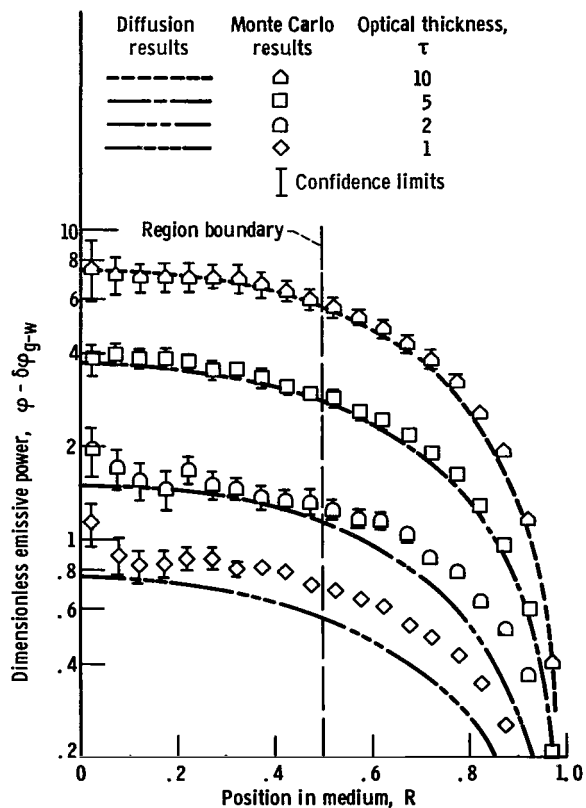
Diffusion results	Monte Carlo results	Optical thickness, τ
----------	△	10
—·—·—	□	5
—··—··—	◁	2
—···—···—	◇	1
	⊥ Confidence limits	

Figure 7. – Dimensionless gas emissive power distribution in gray coaxial regions. Ratio of energy sources, 1; optical thickness in region 1 same as in region 2.
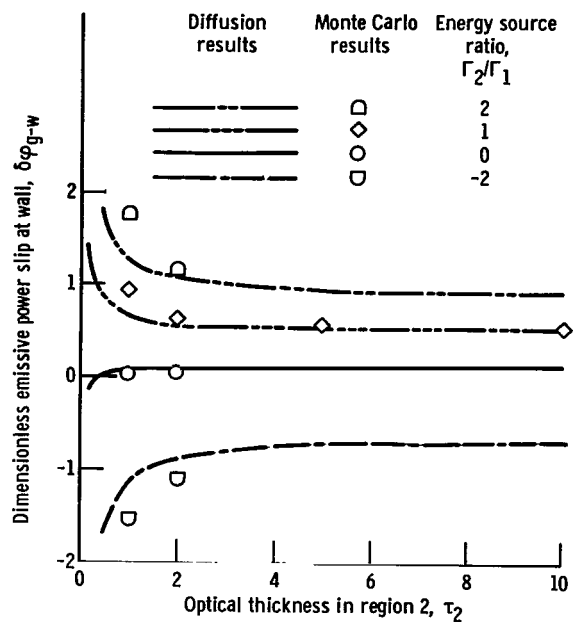
Diffusion results	Monte Carlo results	Energy source ratio, Γ_2/Γ_1
—·—·—	◖	2
—··—··—	◇	1
—···—···—	○	0
—·—·—	◗	-2

Figure 8. – Effect of optical thickness on radiation slip at wall bounding coaxial regions. Ratio of cylinder diameters, 0.5; optical thickness in region 1 same as in region 2.
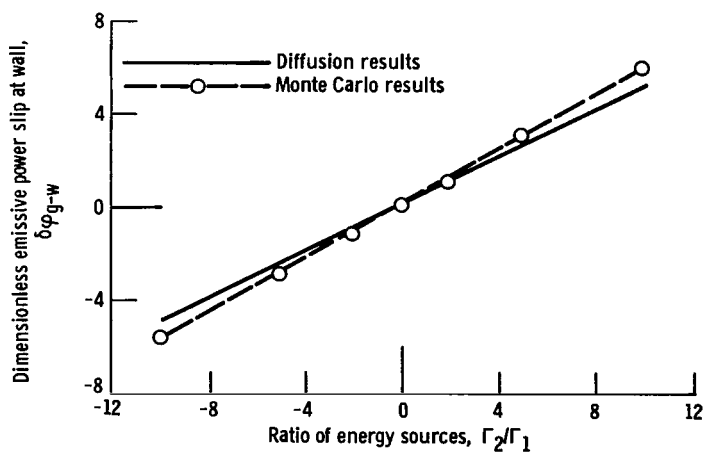

Figure 9. – Effect of energy source ratio on emissive power slip at wall in concentric flow regions. Optical thickness in region 1, 2; optical thickness in region 2, 2; ratio of cylinder diameters, 0.5.
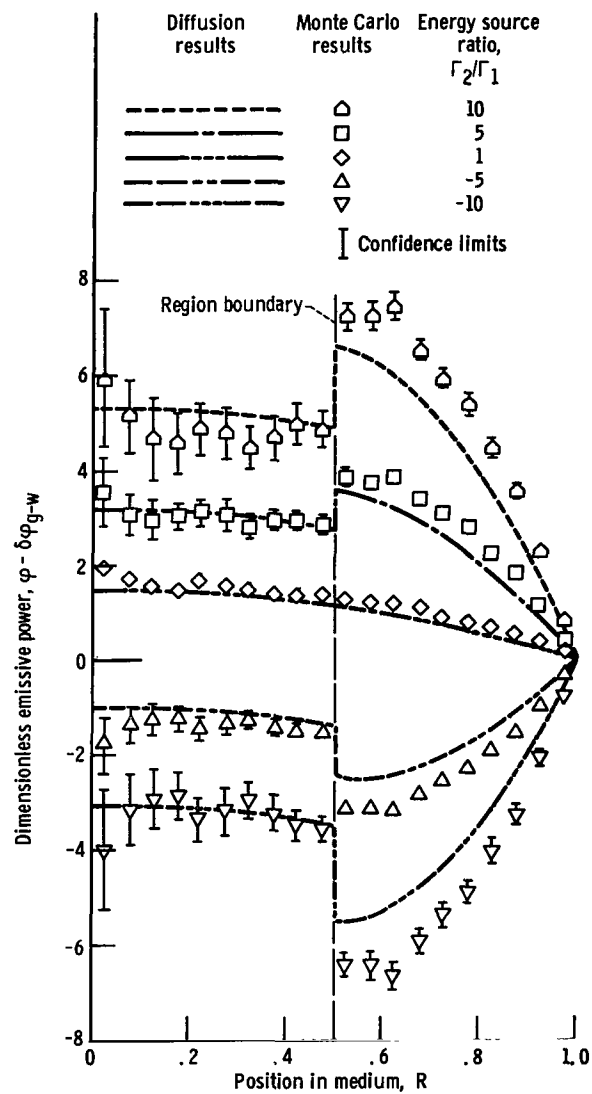
13

Figure 10. – Effect of energy source ratio on emissive power in coaxial regions. Optical thickness in region 1, 2; optical thickness in region 2, 2; ratio of cylinder diameters, 0.5.
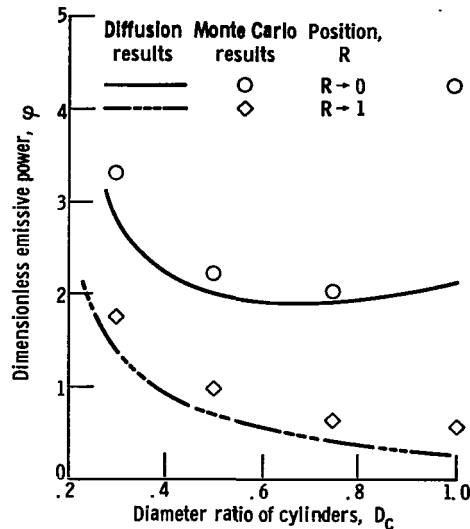
14

Figure 11. - Effect of diameter ratio on emissive power. Energy source ratio, 1; optical thickness in region 1, $10D_c$, where D_c is ratio of cylinder diameters; optical thickness in region 2, $2(1 - D_c)$.

ous state, generating heat internally by the fission process. The heat is transferred to an annulus of flowing propellant, which is then expanded through a nozzle to provide thrust.

The following are the conditions for study based upon some more or less typical conditions (ref. 7). The reactor core has a diameter of 3.2 feet, and the outer diameter of the propellant annulus is 8 feet. Then

$$D_c = \frac{3.2/2}{8/2} = 0.4$$

A fission material of optical thickness $\tau_1 = 10^4$ and a propellant seeded to $\tau_2 = 7$ are used. Also, the propellant flow is adjusted so that 90 percent of the radiant heat generated in the core is absorbed in the propellant. Then

$$0.9\, \Gamma_1 \pi D_c^2 = -\Gamma_2 \pi \left(1 - D_c^2\right)$$

or

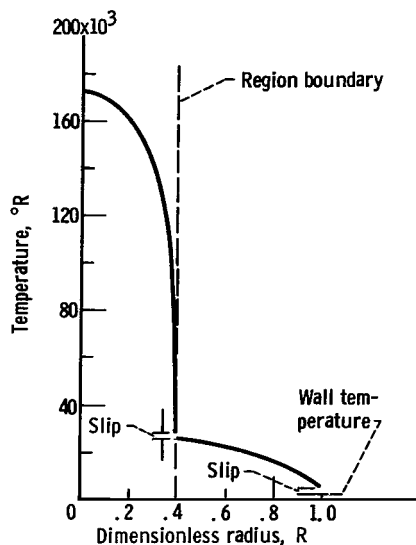$$\frac{\Gamma_2}{\Gamma_1} = -0.172$$

15

Figure 12. - Radial temperature distribution in sample gas-core reactor.

Finally, an emissivity $\epsilon = 0.8$ can be assigned to the bounding surface of the system as a reasonable choice for most metals at high temperature, and the emissive power distribution in the core and propellant regions can be computed by use of equations (A40) to (A43). To find the temperature distribution, the volumetric heat generation rate Γ_1 in region 1 must be specified (eq. (A44)). In the real case, a number such as $\Gamma_1 = 1.4 \times 10^5$ Btu per cubic foot-second is in the region of interest. With this value, the computed temperature distribution is given in figure 12.

In any calculation used in practical design, account must be taken of the property variations with temperature. Allowing κ to vary with temperature in more sophisticated calculations brings the predicted temperatures in the core down to a maximum of about $100\ 000^\circ$ R (ref. 7), which is a considerable change from the prediction of $172\ 000^\circ$ R in this investigation.

The calculation performed herein can be done without a computer and gives an indication of the problems to be expected, that is, the very steep temperature gradient in the fuel near the region boundary and the very high temperatures at the center of the fueled region. The results were calculated by using equations (A40) to (A43) without the necessity of resorting to more complex transport analysis.

CONCLUSIONS

The second-order diffusion solution incorporating jump conditions at region boundaries as proposed by Deissler was extended to problems involving two distinct media,

16

and its region of validity was determined by comparison with a Monte Carlo transport solution.

The emissive power jump that occurs between two absorbing-emitting regions can become important over certain ranges of parameters, and should be examined in any situations where it may exist. The diffusion solution yields accurate answers when applied to problems involving two regions undergoing radiative interchanges of energy, and it can be used over a wider range of parameters than might have been expected. For the problems examined, the diffusion results were within a few percent of the more accurate transport solution so long as the optical thickness in each region was greater than about 1.

Lewis Research Center,
    National Aeronautics and Space Administration,
        Cleveland, Ohio, June 8, 1966,
            129-01-09-09-22.

17

APPENDIX - DIFFUSION SOLUTION

As shown by Deissler (ref. 1), the emissive power of a gas near a point x_0, y_0, z_0 can be expanded in a Taylor series to give

$$e_\lambda = \sum_{n=0}^{\infty} \frac{1}{n!} \left[(z - z_0)\left(\frac{\partial}{\partial z}\right)_0 + (y - y_0)\left(\frac{\partial}{\partial y}\right)_0 + (x - x_0)\left(\frac{\partial}{\partial x}\right)_0 \right]^n e_\lambda \tag{A1}$$

which can be written as

$$e_\lambda = \sum_{n=0}^{\infty} \sum_{v=0}^{n} \sum_{s=0}^{v} \frac{(z - z_0)^{n-v}(y - y_0)^{v-s}(x - x_0)^s}{(n - v)! \, (v - s)! \, s!} \left(\frac{\partial^n e_\lambda}{\partial z^{n-v} \partial y^{v-s} \partial x^s} \right)_0 \tag{A2}$$

By writing equation (A2) in spherical coordinates, applying the equation for emission of energy from an element which arrives at the element of volume around x_0, y_0, z_0 as

$$dE_\lambda = 4\kappa_\lambda e_\lambda \, dV \frac{d\omega}{4\pi} e^{-\kappa_\lambda r}$$

and using these to determine the net flux per unit area per unit frequency interval passing through element dA in direction z, Deissler shows that the net flux is given by

$$q_{\lambda,z} = -\frac{1}{4\pi} \sum_{n=0}^{\infty} \sum_{v=0}^{n} \sum_{s=0}^{v} \left[1 - (-1)^{n-v} \right] \Omega(n, v, s) \frac{1}{\kappa_\lambda^n} \left(\frac{\partial^n e_\lambda}{\partial z^{n-v} \partial y^{v-s} \partial x^s} \right)_0 \tag{A3}$$

where

$$\Omega(n, v, s) = \frac{\left[1 + (-1)^{v-s} \right] \left[1 + (-1)^s \right] n! \, \Gamma\left(\frac{n - v + 2}{2}\right) \Gamma\left(\frac{v - s + 1}{2}\right) \Gamma\left(\frac{s + 1}{2}\right)}{(n - v)! \, (v - s)! \, s! \, \Gamma\left(\frac{n + 4}{2}\right)} \tag{A4}$$

18

The Γ in this equation is the gamma function and is not to be confused with the source strength used elsewhere in this report. For a wall bounding the gas at some positive value of z, the energy jump at the wall is given by

$$e_{\lambda, 0} - e_{\lambda, w} = \left(\frac{1}{\epsilon} - \frac{1}{2}\right) q_{\lambda, z, 0} + \frac{1}{8\pi} \sum_{n=1}^{\infty} \sum_{v=0}^{n} \sum_{s=0}^{v} \left[1 + (-1)^{n-v}\right] \Omega(n, v, s)$$

$$\times \frac{1}{\kappa_\lambda^n} \left(\frac{\partial^n e_\lambda}{\partial z^{n-v} \partial y^{v-s} \partial x^s}\right)_0 \tag{A5}$$

To this point it has only been assumed that the absorption coefficient of the gas does not vary over a mean free path and that the flux solution applies throughout the gas, although it is strictly correct only one mean free path, or more, away from a bounding surface.

If terms with derivatives of higher order than 2 are neglected, equation (A3) reduces to

$$q_{\lambda, z} = -\frac{4}{3\kappa_\lambda} \frac{\partial e_\lambda}{\partial z} \tag{A6}$$

and equation (A5) becomes

$$e_{\lambda, 0} - e_{\lambda, w} = \left(\frac{1}{\epsilon} - \frac{1}{2}\right) q_{\lambda, z, 0} - \frac{1}{2\kappa_\lambda^2} \left(\frac{\partial^2 e_\lambda}{\partial z^2}\right)_0 - \frac{1}{4\kappa_\lambda^2} \left(\frac{\partial^2 e_\lambda}{\partial y^2}\right)_0 - \frac{1}{4\kappa_\lambda^2} \left(\frac{\partial^2 e_\lambda}{\partial x^2}\right)_0 \tag{A7}$$

Writing Planck's spectral distribution function in terms of black emissive power $e_g = \sigma T^4$ rather than in terms of temperature and integrating equations (A6) and (A7) over the wavelength interval $\Delta\lambda$ gives

$$q_{z, \Delta\lambda} = -\frac{4}{3\kappa_{R, \Delta\lambda}} \frac{\partial e_g}{\partial z} \tag{A8}$$

and

19

$$(e_{g,0} - e_w)_{\Delta\lambda} = \left(\frac{1}{\epsilon} - \frac{1}{2}\right)q_{z,0,\Delta\lambda} - \frac{1}{2\kappa_{s,\Delta\lambda}^2}\left(\frac{\partial^2 e_{g,\Delta\lambda}}{\partial z^2}\right)_0 - \frac{I_{\Delta\lambda}}{2}\left(\frac{\partial e_{g,\Delta\lambda}}{\partial z}\right)_0^2$$

$$- \frac{1}{4\kappa_{s,\Delta\lambda}^2}\left(\frac{\partial^2 e_{g,\Delta\lambda}}{\partial y^2}\right)_0 - \frac{I_{\Delta\lambda}}{4}\left(\frac{\partial e_{g,\Delta\lambda}}{\partial y}\right)_0^2 - \frac{1}{4\kappa_{s,\Delta\lambda}^2}\left(\frac{\partial^2 e_{g,\Delta\lambda}}{\partial x^2}\right)_0 - \frac{I_{\Delta\lambda}}{4}\left(\frac{\partial e_{g,\Delta\lambda}}{\partial x}\right)_0^2 \quad \text{(A9)}$$

where

$$\frac{1}{\kappa_{R,\Delta\lambda}} = \frac{\displaystyle\int_{\Delta\lambda} \frac{1}{\kappa_{\lambda,0}}\left(\frac{\partial e_{g,\lambda}}{\partial e_g}\right)_0 d\lambda}{\displaystyle\int_{\Delta\lambda} \left(\frac{\partial e_{g,\lambda}}{\partial e_g}\right)_0 d\lambda} \quad \text{(A10)}$$

$$\frac{1}{\kappa_{s,\Delta\lambda}^2} = \frac{\displaystyle\int_{\Delta\lambda} \frac{1}{\kappa_{\lambda,0}^2}\left(\frac{\partial e_{g,\lambda}}{\partial e_g}\right)_0 d\lambda}{\displaystyle\int_{\Delta\lambda} \left(\frac{\partial e_{g,\lambda}}{\partial e_g}\right)_0 d\lambda} \quad \text{(A11)}$$

and

$$I_{\Delta\lambda} = \frac{\displaystyle\int_{\Delta\lambda} \frac{1}{\kappa_{\lambda,0}^2}\left(\frac{\partial^2 e_{g,\lambda}}{\partial e_g^2}\right) d\lambda}{\left[\displaystyle\int_{\Delta\lambda}\left(\frac{\partial e_{g,\lambda}}{\partial e_g}\right)_0 d\lambda\right]^2} \quad \text{(A12)}$$

To this point, the development is essentially that presented by Deissler (ref. 1) as extended in the discussion appended to reference 1; it differs from the usual diffusion solution chiefly in the retention of second-order terms and in the inclusion of the emissive

power jump (eq. (A9)) at the solid boundary. However, the changes in the results due to these two factors are significant, as is shown by the comparisons in references 1 to 3. These references are for gray gases. When wavelength effects become important, and when κ_λ is a function of temperature, agreement with exact solutions may become less satisfactory, as shown in reference 4.

For the problem at hand, derivation of one more condition is necessary. At the boundary between two regions with different absorption coefficients (fig. 1), the total radiant energy per unit frequency interval passing from region 1 to region 2 through an area dA on the boundary of the regions is

$$dE_{\lambda,1} = \frac{dA}{4\pi} \sum_{n=0}^{\infty} \sum_{v=0}^{n} \sum_{s=0}^{v} (-1)^{n-v} \Omega(n,v,s) \frac{1}{\kappa_{\lambda,1}^{n}} \left(\frac{\partial^n e_\lambda}{\partial z^{n-v} \partial y^{v-s} \partial x^s} \right)_1$$

and from region 2 to region 1 it is

$$dE_{\lambda,2} = \frac{dA}{4\pi} \sum_{n=0}^{\infty} \sum_{v=0}^{n} \sum_{s=0}^{v} \Omega(n,v,s) \frac{1}{\kappa_{\lambda,2}^{n}} \left(\frac{\partial^n e_\lambda}{\partial z^{n-v} \partial y^{v-s} \partial x^s} \right)_2$$

The net radiant flux per unit frequency interval in the z-direction is then

$$q_{\lambda,g-g} = \frac{dE_{\lambda,1} - dE_{\lambda,2}}{dA} = -\frac{1}{4\pi} \sum_{n=0}^{\infty} \sum_{v=0}^{n} \sum_{s=0}^{v} \Omega(n,v,s) \left[\frac{1}{\kappa_{\lambda,2}^{n}} \left(\frac{\partial^n e_\lambda}{\partial z^{n-v} \partial y^{v-s} \partial x^s} \right)_2 \right.$$

$$\left. - (-1)^{n-v} \frac{1}{\kappa_{\lambda,1}^{n}} \left(\frac{\partial^n e_\lambda}{\partial z^{n-v} \partial y^{v-s} \partial x^s} \right)_1 \right]_{g-g} \quad \text{(A13)}$$

Neglecting terms of order higher than 2 and integrating over all wavelengths as before give

$$q_{g\text{-}g} = \left\{ -(e_{g,2} - e_{g,1}) - \frac{2}{3}\left[\frac{1}{\kappa_{R,2}}\left(\frac{\partial e_g}{\partial z}\right)_2 + \frac{1}{\kappa_{R,1}}\left(\frac{\partial e_g}{\partial z}\right)_1 \right] \right.$$

$$+ \frac{1}{2}\left[\frac{1}{\kappa_{s,1}^2}\left(\frac{\partial^2 e_g}{\partial z^2}\right)_1 - \frac{1}{\kappa_{s,2}^2}\left(\frac{\partial^2 e_g}{\partial z^2}\right)_2 \right] + \frac{1}{2}\left[I_1\left(\frac{\partial e_g}{\partial z}\right)_1^2 - I_2\left(\frac{\partial e_g}{\partial z}\right)_2^2 \right]$$

$$+ \frac{1}{4}\left[\frac{1}{\kappa_{s,1}^2}\left(\frac{\partial^2 e_g}{\partial y^2}\right)_1 - \frac{1}{\kappa_{s,2}^2}\left(\frac{\partial^2 e_g}{\partial y^2}\right)_2 \right] + \frac{1}{4}\left[I_1\left(\frac{\partial e_g}{\partial y}\right)_1^2 - I_2\left(\frac{\partial e_g}{\partial y}\right)_2^2 \right]$$

$$\left. + \frac{1}{4}\left[\frac{1}{\kappa_{s,1}^2}\left(\frac{\partial^2 e_g}{\partial x^2}\right)_1 - \frac{1}{\kappa_{s,2}^2}\left(\frac{\partial^2 e_g}{\partial x^2}\right)_2 \right] + \frac{1}{4}\left[I_1\left(\frac{\partial e_g}{\partial x}\right)_1^2 - I_2\left(\frac{\partial e_g}{\partial x}\right)_2^2 \right] \right\}_{g\text{-}g} \tag{A14}$$

For a gray gas, equations (A10) to (A12) give

$$\frac{1}{\kappa_R} = \frac{1}{\kappa_s} \quad \text{and} \quad I = 0$$

Plane Layers

Distribution of emissive power. - If attention is restricted to the model in figure 1(a) and if a gray gas and constant regional properties are assumed, the terms involving derivatives in x and y are zero, and equations (A8), (A9), and (A14) give, respectively,

$$q_z = -\frac{4}{3\kappa}\frac{\partial e_g}{\partial z} \tag{A15}$$

$$e_{g,w} - e_w = \left(\frac{1}{\epsilon} - \frac{1}{2}\right)q_{z,w} - \frac{1}{2\kappa^2}\left(\frac{\partial^2 e_g}{\partial z^2}\right)_w \tag{A16}$$

22

$$(e_{g,2} - e_{g,1})_{g-g} = -q_{z,0} + \left\{ -\frac{2}{3} \left[\frac{1}{\kappa_2} \left(\frac{\partial e_g}{\partial z} \right)_2 + \frac{1}{\kappa_1} \left(\frac{\partial e_g}{\partial z} \right)_1 \right] \right.$$

$$\left. + \frac{1}{2} \left[\frac{1}{\kappa_1^2} \left(\frac{\partial^2 e_g}{\partial z^2} \right)_1 - \frac{1}{\kappa_2^2} \left(\frac{\partial^2 e_g}{\partial z^2} \right)_2 \right] \right\}_{g-g} \tag{A17}$$

In both layers 1 and 2, the net heat flow out of a unit volume must be equal to the volumetric heat generation rate Q minus the rate of change in enthalpy due to flow in the volume. If steady conditions are assumed and flow occurs only in the x-direction, then, for layer 2,

$$\nabla \cdot q_{z,2} = Q_2 - \left(\rho C_p u_x \frac{\partial T}{\partial x} \right)_2 \qquad L_1 \leq z \leq L_2$$

or

$$\frac{4}{3\kappa_2} \frac{\partial^2 e_g}{\partial z^2} = -Q_1 + \left(\rho C_p u_x \frac{\partial T}{\partial x} \right)_1 = -\Gamma_2 \qquad L_1 \leq z \leq L_2 \tag{A18}$$

Putting equation (A18) into dimensionless form gives

$$\frac{\partial^2 e_g}{\partial Z^2} = -\frac{3\tau_2 \Gamma_2 L_2}{4(1 - D)} \qquad D \leq Z \leq 1 \tag{A19}$$

where

$$Z = \frac{z}{L_2}; \quad \tau_2 = \kappa_2 (L_2 - L_1); \quad D = \frac{L_1}{L_2}$$

In region 1, a similar analysis gives

$$\frac{\partial^2 e_g}{\partial Z^2} = -\frac{3\tau_1 \Gamma_1 L_2}{4D} \qquad 0 \leq Z \leq D \tag{A20}$$

23

Integration of equation (A20) with respect to Z gives

$$\frac{\partial e_g}{\partial Z} = -\frac{3\tau_1 \Gamma_1 L_2 Z}{4D} + C_1$$

where C_1 is a constant. However, at $Z = 0$, $(\partial e_g/\partial Z) = 0$ because of the zero flux condition for the model chosen, so that $C_1 = 0$ and

$$\frac{\partial e_g}{\partial Z} = -\frac{3\tau_1 \Gamma_1 L_2 Z}{4D} \qquad 0 \le Z \le D \qquad (A21)$$

Now, integrating equation (A19) with respect to Z gives

$$\frac{\partial e_g}{\partial Z} = -\frac{3\tau_2 \Gamma_2 L_2 Z}{4(1 - D)} + C_2 \qquad D \le Z \le 1 \qquad (A22)$$

To evaluate the constant C_2, it is apparent from equation (A15) that if the radiant flux varies continuously between two regions with different absorption coefficients, then the gradient in emissive power at the boundary between the two regions is related by

$$q_{z,D} = -\frac{4}{3\kappa_1}\left(\frac{\partial e_g}{\partial z}\right)_{1,D} = -\frac{4}{3\kappa_2}\left(\frac{\partial e_g}{\partial z}\right)_{2,D} \qquad (A23a)$$

or, in dimensionless form,

$$\frac{D}{\tau_1}\left(\frac{\partial e_g}{\partial Z}\right)_{1,D} = \frac{1 - D}{\tau_2}\left(\frac{\partial e_g}{\partial Z}\right)_{2,D} \qquad (A23b)$$

Then, combining equation (A22) evaluated at $Z = D$ with equations (A23) and (A21) evaluated at $Z = D$ gives

$$C_2 = -\frac{3\tau_2}{4}\frac{D}{1 - D}L_2(\Gamma_1 - \Gamma_2)$$

and

$$\frac{\partial e_g}{\partial Z} = -\frac{3\tau_2 L_2 \Gamma_2 (Z - D)}{4(1 - D)} - \frac{3\tau_2}{4}\frac{D}{1 - D} L_2 \Gamma_1 \qquad D \le Z \le 1 \qquad \text{(A24)}$$

Integrating once again gives

$$e_g = -\frac{3\tau_2 L_2 \Gamma_2}{4(1 - D)}\left(\frac{Z^2}{2} - DZ\right) - \frac{3\tau_2}{4}\frac{D}{1 - D} L_2 \Gamma_1 Z + C_3 \qquad D \le Z \le 1 \qquad \text{(A25)}$$

The fact that at $Z = 1$ the value of e_g is greater than the emissive power of the wall and will have a value of e_g denoted as $e_{g,w}$ permits evaluation of the constant C_3, and equation (A25) can be written as

$$\varphi_2(Z) - \delta\varphi_{g-w} = \frac{3\tau_2(\Gamma_2/\Gamma_1)(1 - Z^2)}{8D(1 - D)} + \frac{3\tau_2}{4(1 - D)}\left(1 - \frac{\Gamma_2}{\Gamma_1}\right)(1 - Z) \qquad D \le Z \le 1 \qquad \text{(A26)}$$

where

$$\varphi(Z) = \frac{e_g(Z) - e_w}{\Gamma_1 L_1}$$

$$\delta\varphi_{g-w} = \frac{e_{g,w} - e_w}{\Gamma_1 L_1}$$

and e_w is the black emissive power of the bounding surface. The value of $\delta\varphi_{g-w}$ is found directly from equation (A16) by noting that the net flux at the wall $q_{z,w}$ can be obtained from equations (A15) and (A24). Substituting equations (A15), (A24), and (A19) into (A16) and nondimensionalizing give

$$\delta\varphi_{g-w} = \left(\frac{1}{\epsilon} - \frac{1}{2}\right)\left(\frac{1 - D}{D}\frac{\Gamma_2}{\Gamma_1} + 1\right) + \frac{3(\Gamma_2/\Gamma_1)(1 - D)}{8D\tau_2} \qquad \text{(A27)}$$

The value of $e_{g,1,D}$ can be found in terms of $e_{g,2,D}$, which is the emissive power of the gas in region 2 evaluated at point D, and of the discontinuity or jump in emissive power between the two regions. The jump in emissive power at point $Z = D$ can be found from equation (A17) after the emissive power distribution in region 2 is found.

Substituting both the value $\Gamma_1 L_1$ for $q_{z,D}$ and also the appropriate derivatives into equation (A17) and nondimensionalizing give

$$\delta\varphi_{g-g} = \frac{3}{8D}\left(\frac{D}{\tau_1} - \frac{1-D}{\tau_2}\frac{\Gamma_2}{\Gamma_1}\right) \tag{A28a}$$

or, in dimensional form

$$e_{g,1,D} - e_{g,2,D} = \frac{3}{8}\left(\frac{\Gamma_1}{\kappa_1} - \frac{\Gamma_2}{\kappa_2}\right) \tag{A28b}$$

If the regions differ in the magnitudes of either their source strengths or their absorption coefficients, or both, a slip will occur in the gas emissive power at the boundary. The slip will only disappear in the special case $\Gamma_1/\kappa_1 = \Gamma_2/\kappa_2$ or if there is no internal generation in either region.

Now the emissive power distribution in region 1 may be found by integrating equation (A21) and using the slip condition of equation (A28). This gives

$$\varphi_1(Z) - \delta\varphi_{g-w} = \varphi_2(D) - \delta\varphi_{g-w} + \frac{3\tau_1}{8D^2}(D^2 - Z^2) + \delta\varphi_{g-g} \qquad 0 \le Z \le D \tag{A29}$$

The equations for φ in the plane slab geometry are then

$$\varphi_1(Z) - \delta\varphi_{g-w} = \varphi_2(D) - \delta\varphi_{g-w} + \frac{3\tau_1}{8D^2}(D^2 - Z^2) + \delta\varphi_{g-g} \qquad 0 \le Z \le D \tag{A30}$$

$$\varphi_2(Z) - \delta\varphi_{g-w} = \frac{3\tau_2(\Gamma_2/\Gamma_1)}{8D(1-D)}(1 - Z^2) + \frac{3\tau_2}{4(1-D)}\left(1 - \frac{\Gamma_2}{\Gamma_1}\right)(1 - Z) \qquad D \le Z \le 1 \tag{A31}$$

$$\delta\varphi_{g-w} = \left(\frac{1}{\epsilon} - \frac{1}{2}\right)\left(\frac{\Gamma_2}{\Gamma_1}\frac{1-D}{D} + 1\right) + \frac{3(\Gamma_2/\Gamma_1)(1-D)}{8D\tau_2} \tag{A32}$$

$$\delta\varphi_{g-g} = \frac{3}{8D}\left(\frac{D}{\tau_1} - \frac{1-D}{\tau_2}\frac{\Gamma_2}{\Gamma_1}\right) \tag{A33}$$

Energy flux distribution. - Combining equations (A23a) and (A26) gives

$$-q_z = \frac{4(1-D)}{3\tau_2}\left(\frac{\partial e_g}{\partial Z}\right)_w = \frac{4(1-D)}{3\tau_2}\Gamma_1 L_1 \left(\frac{\partial \varphi}{\partial Z}\right)_2$$

$$= \frac{4(1-D)}{3\tau_2}\Gamma_1 L_1 \left[\frac{3\tau_2(\Gamma_2/\Gamma_1)}{4D(1-D)}Z + \frac{3\tau_2}{4(1-D)}\left(1 - \frac{\Gamma_2}{\Gamma_1}\right)\right] \tag{A34}$$

or

$$\psi_2(Z) = -\frac{q_2(Z)}{\Gamma_1 L_1} = \frac{\Gamma_2}{\Gamma_1}\frac{1}{D}Z + 1 - \frac{\Gamma_2}{\Gamma_1}$$

$$= 1 + \frac{\Gamma_2}{\Gamma_1}\left(\frac{Z}{D} - 1\right) \qquad D \leq Z \leq 1 \tag{A35}$$

A similar combination of equation (A23a) evaluated in region 1 and equation (A21) gives

$$\psi_1(Z) = \frac{Z}{D} \qquad 0 \leq Z \leq D \tag{A36}$$

Coaxial Flow Bounded by Cylinder

Emissive power distribution. - For the system shown in figure 1(b), the energy equation may be written as

$$\frac{4}{3\kappa}\frac{1}{r}\frac{d}{dr}\left(r\frac{\partial e_g}{\partial r}\right) = -\Gamma \tag{A37}$$

and (from eq. (A9)) the emissive power jump at the wall can be written as

$$e_{g,w} - e_w = \left(\frac{1}{\epsilon} - \frac{1}{2}\right)q_{z,w} - \frac{1}{2\kappa_2^2}\left(\frac{\partial^2 e_g}{\partial z^2}\right)_w - \frac{1}{2\kappa_2^2}\left(\frac{\partial^2 e_g}{\partial y^2}\right)_w \tag{A38}$$

The emissive power jump at the boundary between regions is

$$(e_{g,1} - e_{g,2})_{g-g} = q_D + \frac{2}{3}\left[\frac{1}{\kappa_1}\left(\frac{\partial e_g}{\partial z}\right)_1 + \frac{1}{\kappa_2}\left(\frac{\partial e_g}{\partial z}\right)_2\right] + \frac{1}{2}\left[\frac{1}{\kappa_1^2}\left(\frac{\partial^2 e_g}{\partial z^2}\right)_1 - \frac{1}{\kappa_2^2}\left(\frac{\partial^2 e_g}{\partial z^2}\right)_2\right]$$

$$+ \frac{1}{4}\left[\frac{1}{\kappa_1^2}\left(\frac{\partial^2 e_g}{\partial y^2}\right)_1 - \frac{1}{\kappa_2^2}\left(\frac{\partial^2 e_g}{\partial y^2}\right)_2\right] \quad \text{(A39)}$$

By following a derivation similar to that for plane layers, and noting that r in the equations must be replaced by $(z^2 + y^2)^{1/2}$ in the evaluation of derivatives, it is evident that

$$\varphi_1(R) - \delta\varphi_{g-w} = \varphi_2(D_c) - \delta\varphi_{g-w} + \delta\varphi_{g-g} + \frac{3\tau_1}{16}\frac{D_c^2 - R^2}{D_c^2} \quad 0 \le R \le D_c \quad \text{(A40)}$$

$$\varphi_2(R) - \delta\varphi_{g-w} = \frac{3\tau_2}{16}\frac{\Gamma_2}{\Gamma_1}\frac{1 - R^2}{D_c(1 - D_c)} - \frac{3\tau_2 D_c}{8(1 - D_c)}\left(1 - \frac{\Gamma_2}{\Gamma_1}\right)\ln R \quad D_c \le R \le 1 \quad \text{(A41)}$$

where

$$\delta\varphi_{g-w} = \frac{1}{2}\left(\frac{1}{\epsilon} - \frac{1}{2}\right)\left(\frac{\Gamma_2}{\Gamma_1}\frac{1 - D_c^2}{D_c} + D_c\right) + \frac{3}{16}\frac{1 - D_c}{\tau_2}\left(\frac{\Gamma_2}{\Gamma_1}\frac{1 + D_c^2}{D_c} - D_c\right) \quad \text{(A42)}$$

$$\delta\varphi_{g-g} = \frac{9}{32D_c}\left[\frac{D_c}{\tau_1} - \frac{1}{3}\frac{1 - D_c}{\tau_2}\left(4\frac{\Gamma_2}{\Gamma_1} - 1\right)\right] \quad \text{(A43)}$$

where

$$R = \frac{r}{r_2}; \quad \varphi(Z) = \frac{e_g(Z) - e_w}{\Gamma_1 r_1}; \quad D_c = \frac{r_1}{r_2}; \quad \tau_1 = \kappa_1 r_1; \quad \tau_2 = \kappa_2(r_2 - r_1)$$

28

Energy flux distribution. - By analysis similar to that for the plane geometry, the energy flux distribution is found to be

$$\psi_1(R) = \frac{R}{2D_c} \quad 0 \le R \le D_c \tag{A44}$$

$$\psi_2(R) = \frac{D_c}{2R} + \frac{\Gamma_2}{\Gamma_1}\frac{R^2 - D_c^2}{2RD_c} \quad D_c \le R \le 1 \tag{A45}$$

REFERENCES

1. Deissler, R. G.: Diffusion Approximation for Thermal Radiation in Gases with Jump Boundary Condition. J. Heat Transfer, vol. 86, no. 2, May 1964, pp. 240-246.

2. Howell, J. R.; and Perlmutter, M.: Monte Carlo Solution of Thermal Transfer Through Radiant Media Between Gray Walls. J. Heat Transfer, vol. 86, no. 1, Feb. 1964, pp. 116-122.

3. Perlmutter, M.; and Howell, J. R.: Radiant Transfer Through a Gray Gas Between Concentric Cylinders Using Monte Carlo. J. Heat Transfer, vol. 86, no. 2, May 1964, pp. 169-179.

4. Howell, John R.: Calculation of Radiant Heat Exchange by the Monte Carlo Method. Paper No. 65-WA/HT-54, ASME, Nov. 1965.

5. Einstein, Thomas H.: Radiant Heat Transfer to Absorbing Gases Enclosed in a Circular Pipe with Conduction, Gas Flow, and Internal Heat Generation. NASA TR R-156, 1962.

6. Howell, J. R.: On the Radiation Slip Between Absorbing-Emitting Regions with Heat Sources. (Submitted to International J. Ht. and Mass Trans.)

7. Cooper, Ralph S., comp.: Proceedings of an Advanced Nuclear Propulsion Symposium. Rep. No. LA-3229, Los Alamos Scientific Lab., Jan. 1965.

"The aeronautical and space activities of the United States shall be conducted so as to contribute . . . to the expansion of human knowledge of phenomena in the atmosphere and space. The Administration shall provide for the widest practicable and appropriate dissemination of information concerning its activities and the results thereof."

—NATIONAL AERONAUTICS AND SPACE ACT OF 1958

NASA SCIENTIFIC AND TECHNICAL PUBLICATIONS

TECHNICAL REPORTS: Scientific and technical information considered important, complete, and a lasting contribution to existing knowledge.

TECHNICAL NOTES: Information less broad in scope but nevertheless of importance as a contribution to existing knowledge.

TECHNICAL MEMORANDUMS: Information receiving limited distribution because of preliminary data, security classification, or other reasons.

CONTRACTOR REPORTS: Technical information generated in connection with a NASA contract or grant and released under NASA auspices.

TECHNICAL TRANSLATIONS: Information published in a foreign language considered to merit NASA distribution in English.

TECHNICAL REPRINTS: Information derived from NASA activities and initially published in the form of journal articles.

SPECIAL PUBLICATIONS: Information derived from or of value to NASA activities but not necessarily reporting the results of individual NASA-programmed scientific efforts. Publications include conference proceedings, monographs, data compilations, handbooks, sourcebooks, and special bibliographies.

Details on the availability of these publications may be obtained from:

SCIENTIFIC AND TECHNICAL INFORMATION DIVISION

NATIONAL AERONAUTICS AND SPACE ADMINISTRATION

Washington, D.C. 20546